Sensors & Diagnostics

PAPER

View Article Online
View Journal | View Issue

Cite this: *Sens. Diagn.*, 2022, **1**, 294

Organic photoelectrochemical transistor detection of tear lysozyme†

Zheng Li,[a] Jin Hu,[a] Ge Gao,[a] Xiang-Nan Liu,[a] Jia-Qi Wu,[a] Yi-Tong Xu,[a] Hong Zhou,[b] Wei-Wei Zhao,*[a] Jing-Juan Xu*[a] and Hong-Yuan Chen*[a]

Received 21st December 2021,
Accepted 27th January 2022

DOI: 10.1039/d1sd00074h

rsc.li/sensors

Rational utilization of rich interplay between light and materials taking place in an organic electrochemical transistor (OECT) is emerging and gaining more interest from the scientific community. Light modulation is expected to realize the advanced organic photoelectrochemical transistor (OPECT) with better performance. A tear holds great potential for biodetection as it contains many biomarkers of physiological importance. In this work, we introduce a novel OPECT towards detection of a tear biomarker, which is demonstrated by assembling CdS quantum dots (QDs) onto a metallic Ti wire followed by assembly of specific aptamers toward a model target of lysozyme. Upon light illumination, the alternation of the potential drop at the CdS QDs/Ti gate electrode surface induced by biorecognition could intimately change the doping/de-doping status of the poly(3,4-ethylenedioxythiophene):poly(styrene sulfonate) (PEDOT:PSS), resulting in amplified channel current signals for sensitive lysozyme detection. This work provides a new and simple platform for detection of a tear biomarker and beyond.

Introduction

Photoelectrochemical (PEC) bioanalysis, established upon the photon-to-electricity conversion of various semiconductive materials, represents an actively developing technology for advanced bioanalytics.[1–8] The separation and the different energy forms of the input (light) and the output (electricity) make this methodology have reduced background and higher sensitivity. To date, numerous materials and signaling strategies have been exploited in this field,[9–12] and the as-developed biosensors have been widely applied ranging from macroscopic *in vitro* detection to nanoscopic *in vivo* measurement.[13–18] For example, Zhang *et al.* designed photonic–plasmonic synergistic resonators in the second near-infrared window for PEC biodetection.[13] Our group developed an integrated PEC nanotool for single-cell drug delivery and assessment of the corresponding treatment effect.[14]

Organic electrochemical transistors (OECTs),[19–24] involving electrochemical doping/de-doping, represent another rapidly developing detection technology due to their attractive properties, *e.g.*, miniaturized structure, intrinsic signal amplification, and compatibility for aqueous operation, which are necessary for biodetection. A typical OECT consists of a thin organic semiconductor, *e.g.*, conducting polymer poly(3,4-ethylenedioxythiophene):poly(styrene sulfonate) (PEDOT:PSS), coated on the channel (C) between the drain (D) electrode and the source (S) electrode, and a gate (G) electrode immersed with an electrolyte (E). Principally, any small potential change at an interface can cause a considerable change of the channel current, making the OECT highly sensitive in transducing biochemical species. Targeting clinically relevant analytes, to date, OECT biosensors have been used for sensing in breath,[25] sweat,[26] saliva,[27] urine,[28] and blood,[29] and, nevertheless, have not been applied for tears.

Based upon the elegant synergy between the OECT and PEC bioanalyses, the concept of an organic photoelectrochemical transistor (OPECT) has recently been proposed.[30] On the basis of the interaction between light and a photoactive G-electrode, the physicochemical rationale of an OPECT is that the light-induced potential change at the G/E interface can regulate the doping/de-doping status of C and thus lead to the potential change at the C/E interface for amplified signaling. Inheriting the advantages of both the PEC and OECT sides, our recent study has revealed the sensitive OPECT biodetection at zero gate bias.[31] Given the merits of non-contact light stimuli and rich light-matter interplay, much remains to be learned and done.

A tear, produced by lacrimal glands, contains many biospecies of physiological significance, *e.g.*, potassium, lactate, glucose and proteins. Compared with blood, it offers

[a] *State Key Laboratory of Analytical Chemistry for Life Science, School of Chemistry and Chemical Engineering, Nanjing University, Nanjing 210023, China. E-mail: zww@nju.edu.cn, xujj@nju.edu.cn, hychen@nju.edu.cn*
[b] *Shandong Key Laboratory of Biochemical Analysis, College of Chemistry and Molecular Engineering, Qingdao University of Science and Technology, Qingdao 266042, China*

† Electronic supplementary information (ESI) available. See DOI: 10.1039/d1sd00074h

a rather clean background and thus holds great potential for simple and fast detection. Current commercial techniques established for tear biomarkers include the enzyme-linked immunosorbent assay (ELISA),[32] Advanced Tear Diagnostic Test Kit[33] and InflammaDry.[34] Although every approach has obvious advantages, each also suffers from its own limitations such as specialized equipment, high cost or complicated procedures.[35] Hence, new cost-effective and user-friendly technologies towards tear detection are still of urgent need. Given the potential of the OPECT, we envision that it could serve as a new platform for tear detection, which might be helpful in future diagnosis of ocular and other diseases.

With these motivations, herein we describe the OPECT detection of a tear biomarker, which to our knowledge has not been reported. Fig. 1a and b schematically illustrate a PEDOT:PSS-based device and a G-electrode of a titanium (Ti) wire functionalized with CdS quantum dots (QDs) and a specific aptamer towards a model target of lysozyme, a natural antibacterial protein existing in various body fluids and also a representative tear biomarker of chronic dry eye syndrome. In the detection, the aptamer would confine the target onto the gate surface, leading to a change of surface potential and the de-doping status of the C and ultimately the amplified signal alternation. This protocol is demonstrated to be both simple and accurate while achieving a sensitive and rapid responsiveness. The detailed fabrication, characterization, performance characteristics, and corresponding mechanism explanation of the OPECT biosensor are described in the following sections.

Experimental section

Reagents and materials

All the reagents were supplied from formal commercial suppliers and were used without any further purification. For the experimental details about the synthesis, fabrication and data acquisition, please refer to the ESI.†

Aptamer immobilization

The aptamers were immobilized onto a CdS QDs/Ti G-electrode *via* an amide bond, and the amino groups on the aptamer and carboxyl groups on CdS QDs were coupled. Firstly, the solution containing 20 mg mL^{-1} EDC and 10 mg

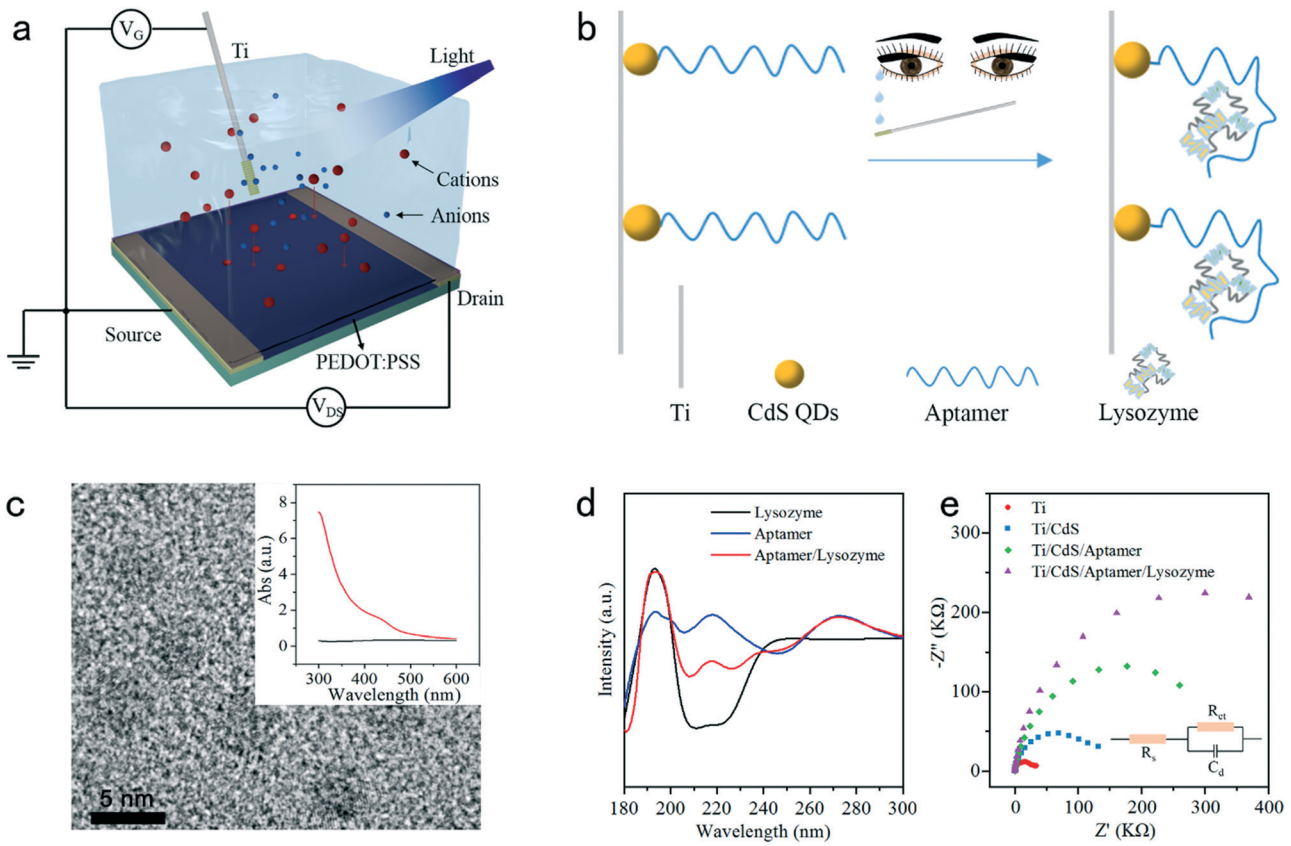

Fig. 1 (a) Schematic of the proposed biosensor. (b) Schematic illustration of the CdS QDs/aptamer-functionalized G-electrode for lysozyme in tear probing. (c) TEM images of the synthesized CdS QDs. Inset: The UV-vis absorption spectra (black curve) before and (red curve) after surface modification of CdS QDs. (d) CD spectra of the aptamer before and after binding with lysozyme. (e) Electrochemical impedance spectroscopy (EIS) of the Ti G-electrode with four different states (only Ti, modification of CdS QDs, immobilization of the aptamer, and combination of lysozyme), which is measured in 0.1 M KCl containing a redox probe of a 5.0 mM $K_3[Fe(CN)_6]/K_4[Fe(CN)_6]$ (1 : 1) mixture. The inset shows the corresponding equivalent circuit.

mL^{-1} NHS was used to treat the as-prepared CdS QDs/Ti G-electrode for 50 min at room temperature. After washing with PBS carefully, 10 μL aptamer solution (0.1 μM concentration) was added to a centrifuge tube with a capacity of 200 μL, and then the CdS QDs/Ti G-electrode was soaked in the aptamer solution and incubated at 4 °C for 12 h. Subsequently, the G-electrode was cleaned with PBS solution to remove the non-immobilized DNA probes. Then, the excess carboxyl groups of CdS QDs were blocked by 1 mM MEA at 4 °C for 2 h. Finally, PBS solution was employed to rinse the G-electrode carefully.

Lysozyme detection

For the lysozyme detection, 10 μL lysozyme targets with different concentrations were added to a centrifuge tube with a capacity of 200 μL, and then the G-electrode which immobilized the aptamer was immersed into the lysozyme solution for 1 h incubation at 37 °C. Afterwards the uncombined lysozyme targets should be washed away using the PBS solution (3 times). To determine the specificity for lysozyme detection, the aptamer/CdS QDs/Ti gate electrode was incubated with 2 μg mL^{-1} lysozyme and 100 μg mL^{-1} IgG, IgA, BSA, and HAS, respectively.

Results and discussion

To be used as a biosensor, the PEDOT:PSS-based device should be very stable in electrolyte. The device was prepared and then characterized in phosphate-buffered saline (PBS) solution containing 0.1 M ascorbic acid for 2000 min to study the device stability. Ag/AgCl is initially chosen as the G-electrode since there is no capacitance associated with faradic current at its interface.[36] As shown in Fig. S1,† the transfer characteristic curves measured from 5 min to 2000 min were quite consistent, indicating the excellent stability of the as-fabricated OECT device. The subsequent measurement of the output characteristic curves, as recorded in Fig. S2,† reflected the sensitive response of the device toward varying V_G values. Fig. S3† shows the operational stability of the channel current response of the device upon applying varying potential steps from 0.1 V to 0.5 V. As shown, the current responses were recorded as the potential was repeatedlty switched on and off more than 25 times over 1000 s, and the device generated reproducible signal responses without any noticeable decrease within this period. On the other hand, the CdS QDs/Ti electrode was also fabricated and characterized. As shown in Fig. 1c, the size of the as-prepared CdS QDs corresponded to *ca.* 5 ± 1 nm as shown by transmission electron microscopy (TEM) measurements. The successful fabrication of the CdS QDs/Ti G-electrode was verified using the UV-vis absorption spectrum. As shown in the inset in Fig. 1c, the pristine Ti electrode did not exhibit any absorption within the visible range (black curve), whereas prominent absorption emerged for the CdS QD-modified Ti electrode in the same range (red curve). The stability of the CdS QDs/Ti G-electrode was then studied *via* time-based photocurrent response. As shown in Fig. S4,† following the onset of light irradiation, the fast rise of signal indicated the efficient charge excitation, separation, and transfer and good electrical contact between the CdS QDs and the Ti substrate as the current collector. The light-controlled generation of reproducible photocurrent also suggested its high photophysical stability.

Circular dichroism (CD) spectra were used to characterize the structural changes of the aptamer and after incubation with lysozyme. As depicted in Fig. 1d, the aptamer is a typical B-form DNA, which has a positive long wavelength band around 260–280 nm and a negative band at about 245 nm (blue curve).[37] The shape of lysozyme is approximately elliptical, and its conformation is complex;[38] two negative bands near 208 and 222 nm are the key to determining the secondary structure of lysozyme (black curve).[39] After incubation with the aptamer, the CD spectrum has significantly changed at *ca.* 208 and 222 nm, implying the combination of the aptamer and lysozyme (red curve). The developmental process of the aptamer/CdS QDs/Ti G-electrode and its recognition with lysozyme were subsequently monitored by electrochemical impedance spectroscopy (EIS), which is an effective technique to characterize the interface properties. In the Nyquist plot, an increase in the diameter of the resistance circle means a decrease in the charge-transfer ability between the electrode and solution. As shown in Fig. 1e, both bare Ti and CdS QDs/Ti exhibited a small semicircle. Subsequently, with the modification with the aptamer and lysozyme, the diameter of the semicircle increased. The inset in Fig. 1e shows the corresponding equivalent circuit. Incidentally, as shown in Fig. S5,† the above-mentioned developmental process was also confirmed using an atomic force microscope (AFM), and the aptamer concentration was optimized to be 0.1 μM to modify the CdS QDs/Ti electrode for subsequent application, as shown in Fig. S6.†

The PEDOT:PSS-based device was then assembled with the aptamer/CdS QDs/Ti G-electrode to construct the proposed device to detect the tear biomarker lysozyme. In the present case, the light-induced electrochemical doping/de-doping of the PEDOT film underpins the working mechanism of the OECT.[30] Specifically, the doping/de-doping process could be described with the electrochemical reaction as follows:[40,41]

$$n(\mathrm{PEDOT^+{:}PSS^-}) + \mathrm{M}^{n+} + ne^- \leftrightarrow n\mathrm{PEDOT}^0 + \mathrm{M}^{n+}{:}n\mathrm{PSS}^- \quad (1)$$

where n is the number of charges of the cation, and M^{n+} is the cation in the electrolyte. When the gate voltage is applied, the cation in the electrolyte will migrate to the $PEDOT^+:PSS^-$ film and thus lead to reduction from the high conductivity state ($PEDOT^+$) to the neutral state ($PEDOT^0$). Initially, the regulation performance of the aptamer/CdS QDs/Ti G-electrode on the transistor was studied. As shown in Fig. 2a, in the absence of light illumination, the transfer characteristic curve of the integrated device was measured (black dotted curve). In the presence of light illumination, the transfer characteristic curve moved obviously to lower voltages (red curve). As illustrated in Fig. 2b, both solid–liquid interfaces have an electric double layer

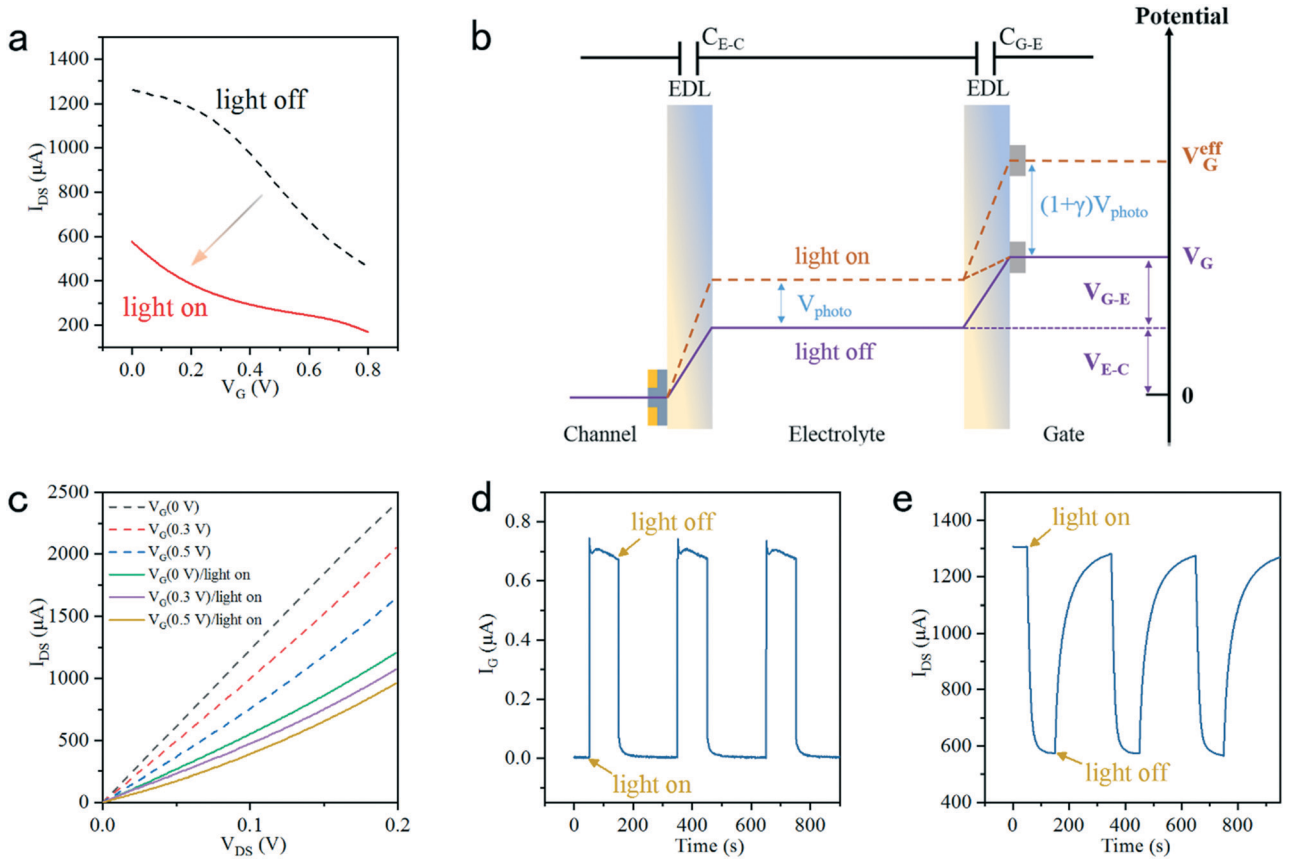

Fig. 2 (a) The $I_{DS} \sim V_G$ curves of the biosensor measured in 0.1 M AA solution before (black dotted curve) and after (red curve) light illumination. V_{DS} = 0.1 V. (b) The variations in potential distribution of the gate voltage applied on the biosensor and the photovoltage V_{photo} induced by light illumination. (c) The $I_{DS} \sim V_{DS}$ curves of the biosensor measured in AA solution before (dotted curves) and after (solid curves) light illumination. V_G = 0 V, 0.3 V, and 0.5 V. (d) The time dependence of I_G at three light off/on cycles. (e) The corresponding time dependence of I_{DS} of the biosensor with three light off/on cycles at zero gate bias. V_{DS} = 0.1 V.

(EDL), which can be regarded as two capacitors in series. Without the light illumination, the gate potential is distributed to the two capacitors, *i.e.*, gate/electrolyte and electrolyte/channel capacitors.[42] V_{E-C} could be given by:

$$V_{E-C} = V_G - V_{G-E} = \frac{V_G}{1+\gamma}$$

$$\gamma = \frac{C_{E-C}}{C_{G-E}} \quad (2)$$

where V_{G-E} and V_{E-C} are the potential distributed on the as-mentioned two solid–liquid interfaces. C_{G-E} and C_{E-C} are the corresponding capacitances of the two EDLs. By contrast, under light illumination, as shown in Fig. S7,† the electron on the conduction band (CB) of CdS QDs transferred to the Ti G-electrode, which can lead to the decrease of the potential drop of C_{G-E}, and V_{photo} is defined as the value where the potential drop varies.[30] For the change in V_{E-C} caused by light irradiation, which is V'_{E-C}, the effective gate voltage V_G^{eff} could be calculated using:

$$V'_{E-C} = \frac{V_G}{1+\gamma} + V_{photo}$$

$$V_G^{eff} = V_G + (1+\gamma)V_{photo} \quad (3)$$

which well explained the shift of the transfer characteristic curve under light irradiation.

Fig. 2c shows the output I_{DS} at varying V_G values (0 V, 0.3 V and 0.5 V) with light on and off. The I_{DS} could be given by:[36,43]

$$I_{DS} = \frac{q\mu p_0 tW}{LV_P}\left(V_P - V_G^{eff} + \frac{V_{DS}}{2}\right)V_{DS} \left(|V_{DS}| \ll |V_P - V_G^{eff}|\right)$$

$$V_P = \frac{qp_0 t}{c_i}$$

$$V_G^{eff} = V_G + V_{offset} \quad (4)$$

where q, μ and p_0 are the electronic charge, the hole mobility and the initial hole density, respectively. t, W and L are the thickness, width and length of the OECT device channel

organic semiconductor film, respectively; c_i denotes the effective capacitance per unit area of the transistor; V_P indicates the pinch-off voltage. V_{offset} is the offset voltage at two capacitances. Together eqn (3) and (4) could easily explain the decrease in I_{DS} under light irradiation. Fig. 2d shows the time-dependent gate current I_G at several intermittent light on/off cycles, with the simultaneous I_{DS} behavior as shown in Fig. 2e. As shown in Fig. S8,† the I_{DS} responses of six aptamer/CdS QDs/Ti G-electrodes fabricated in the same batch confirmed a good repeatability, with highly identical current signals caused by light irradiation. The change in the channel current value (I_{step}) at a cycle of light on and off could be calculated using:

$$I_{step} = I_{DS}^{off} - I_{DS}^{on} \quad (5)$$

where I_{DS}^{off} and I_{DS}^{on} is the channel current value when light was off and on, respectively. Note that the I_{step} response is of several hundred μA, and the corresponding I_G response is of only a few μA.

Fig. 3a recorded the stepwise I_{DS} responses during the system development, *i.e.*, the signals of the pristine CdS QD-modified Ti G-electrode (curve a), after modification with the aptamer (curve b) and further combination with lysozyme (curve c). It can be found that the CdS QD-modified Ti G-electrode enabled the maximum I_{step}, which exhibited a decrease after the immobilization of the aptamer. After further combination of the aptamer with lysozyme, I_{step} further decreased. $\Delta I/I$ was employed as the signal response, which could be calculated using:

$$\Delta I/I = \frac{I_{step}^{aptamer} - I_{step}^{lysozome}}{I_{step}^{aptamer}} \quad (6)$$

where $I_{step}^{aptamer}$ and $I_{step}^{lysozyme}$ correspond to current responses after the modification with the aptamer and the lysozyme recognition, respectively. A linear relationship can be derived for the measurement of lysozyme in the concentration region from 2×10^{-9} to 2×10^{-4} g mL^{-1}, as shown in Fig. 3b. The value of $\Delta I/I$ was 1.15%, which corresponded to pure PBS (baseline noise), and hence the detection limit (the signal response was three times higher than the baseline noise) can reach 5.5×10^{-10} g mL^{-1}. In order to confirm the selectivity, Fig. 3c shows the selectivity to three proteins, namely,

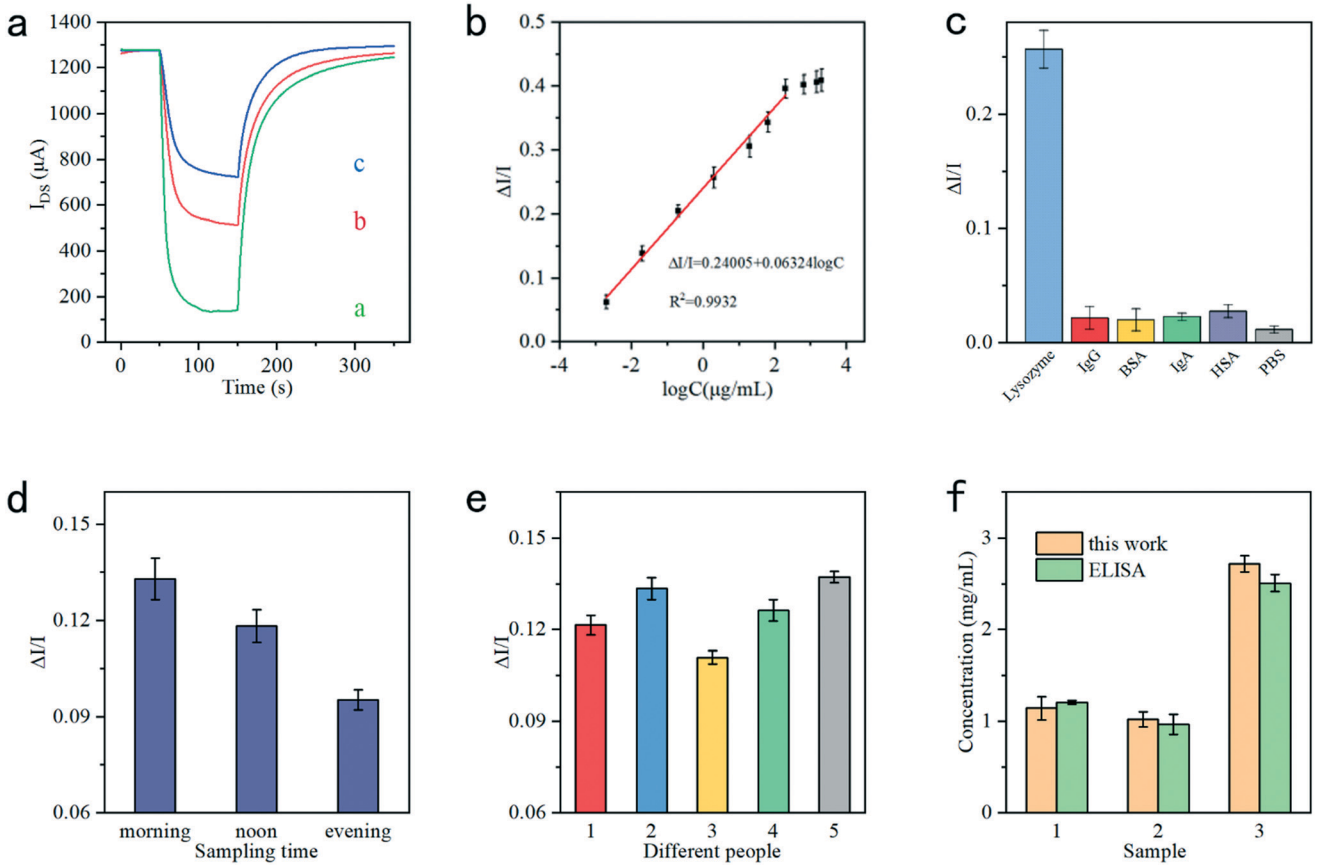

Fig. 3 (a) Channel current I_{DS} response of (curve a) the CdS QDs/Ti G-electrode and the electrode after (curve b) modification with the 0.1 μM aptamer and blocked by 1 mM MEA and (curve c) combination with 2 μg mL^{-1} lysozyme. V_G = 0 V, V_{DS} = 0.1 V. (b) The corresponding derived calibration curve. $\Delta I/I$ as a function of lysozyme concentration. (c) The selectivity of the prepared biosensor. The concentration of lysozyme and other proteins are 2 μg mL^{-1} and 100 μg mL^{-1}, respectively. (d) The $\Delta I/I$ response to the tears sampled by the same person in the morning, noon and evening (the samples were diluted 10^5-fold). (e) The $\Delta I/I$ response to the tears sampled by different people (the samples were diluted 10^5-fold). (f) Quantitative analysis of the concentration of lysozyme in tears sampled by different people through the biosensor and ELISA.

immuno-globulin G (IgG), immune-globulin A (IgA) and human serum albumin (HSA) that exist in tears and one common protein, bovine serum albumin (BSA), as interference to study. The concentrations of these four interfering proteins were 50 times higher than that of lysozyme, and the $\Delta I/I$ was very close to that of the blank test in PBS, indicating the favourable selectivity. The analysis of the real tear sample was then carried out. The tears sampled by the same person in the morning, noon and evening were detected using the biosensor, and as shown in Fig. 3d, the results indicated that the concentrations of lysozyme varied in different periods. Fig. 3e shows that different people have different levels of lysozyme in tears, but most of the test results were in the range of 1–3 mg mL^{-1}.[35,44,45] The accuracy of this method was then compared with that of ELISA, and the results were consistent with each other, as shown in Fig. 3f and S9.† Together these results demonstrated the potential of this method for practical tear biomarker detection.

Conclusion

In short, we have engineered a new OPECT platform towards detection of tear biomarkers. The sensing mechanism of the device can be attributed to the target-dependent change of the surface potential drop, influencing the doping/de-doping status of PEDOT:PSS and thus the current responses. In the lysozyme detection, the device exhibited high selectivity and sensitivity due to the specificity of the aptamer and the intrinsic signal amplification of the device. We expect that this study has implications not only for the structural design of light-sensitive OPECT devices, but also for development of practical OPECT biosensors towards detection of other tear biomarkers and beyond.

Conflicts of interest

There are no conflicts to declare.

Acknowledgements

We thank the National Natural Science Foundation of China (Grant No. 21974059, 22034003, and 22174063) and the Excellent Research Program of Nanjing University (ZYJH004).

References

1 W. W. Zhao, J. J. Xu and H. Y. Chen, *Chem. Rev.*, 2014, **114**, 7421–7441.
2 W. W. Zhao, J. J. Xu and H. Y. Chen, *Chem. Soc. Rev.*, 2015, **44**, 729–741.
3 R. J. Zeng, W. J. Wang, G. N. Cai, Z. L. Huang, J. M. Tao, D. P. Tang and C. Z. Zhu, *Nano Energy*, 2020, **74**, 104931.
4 S. Y. Tang, C. C. Yang, T. Y. Su, T. Y. Yang, S. C. Wu, Y. C. Hsu, Y. Z. Chen, T. N. Lin, J. L. Shen, H. N. Lin, P. W. Chiu, H. C. Kuo and Y. L. Chueh, *ACS Nano*, 2020, **14**, 12668–12678.
5 T. S. Metzger, C. G. Chandaluri, R. Tel-Vered, R. Shenhar and I. Willner, *Adv. Funct. Mater.*, 2016, **26**, 7148–7155.
6 Y. Qin, J. Wen, L. R. Zheng, H. Y. Yan, L. Jiao, X. S. Wang, X. L. Cai, Y. Wu, G. J. Chen, L. J. Chen, L. Y. Hu, W. L. Gu and C. Z. Zhu, *Nano Lett.*, 2021, **21**, 1879–1887.
7 K. Zhao, X. Q. Yan, Y. S. Gu, Z. Kang, Z. M. Bai, S. Y. Cao, Y. C. Liu, X. H. Zhang and Y. Zhang, *Small*, 2016, **12**, 245–251.
8 X. X. Ye, X. Wang, Y. Kong, M. J. Dai, D. X. Han and Z. H. Liu, *Angew. Chem., Int. Ed.*, 2021, **60**, 11774–11778.
9 X. X. Zeng, W. W. Tu, J. Li, J. C. Bao and Z. H. Dai, *ACS Appl. Mater. Interfaces*, 2014, **6**, 16197–16203.
10 H. Dai, S. P. Zhang, Z. S. Hong and Y. Y. Lin, *Anal. Chem.*, 2016, **88**, 9532–9538.
11 R. Y. Yang, K. Zou, X. H. Zhang, C. C. Du and J. H. Chen, *Biosens. Bioelectron.*, 2019, **132**, 55–61.
12 C. G. Hu, J. N. Zheng, X. Y. Su, J. Wang, W. Z. Wu and S. S. Hu, *Anal. Chem.*, 2013, **85**, 10612–10619.
13 B. H. Fu and Z. H. Zhang, *Nano Lett.*, 2019, **19**, 9069–9074.
14 Y. F. Ruan, F. Z. Chen, Y. T. Xu, T. Y. Zhang, S. Y. Yu, W. W. Zhao, D. C. Jiang, H. Y. Chen and J. J. Xu, *Angew. Chem., Int. Ed.*, 2021, **60**, 25762–25765.
15 X. Li, X. L. Wang, L. Zhang and J. M. Gong, *ACS Sens.*, 2018, **3**, 1480–1488.
16 F. Z. Chen, Z. Li, X. N. Liu, Y. C. Zhu, D. M. Han and H. Y. Chen, *Anal. Chem.*, 2021, **93**, 5001–5004.
17 J. H. Feng, N. Li, Y. Du, X. Ren, X. Y. Wang, X. J. Liu, H. M. Ma and Q. Wei, *Anal. Chem.*, 2021, **93**, 14196–14203.
18 Y. H. Xiang, Y. Kong, W. Q. Feng, X. X. Ye and Z. H. Liu, *Chem. Sci.*, 2021, **12**, 12977–12984.
19 P. Schmode, D. Ohayon, P. M. Reichstein, A. Savva, S. Inal and M. Thelakkat, *Chem. Mater.*, 2019, **31**, 5286–5295.
20 P. R. Paudel, V. Kaphle, D. Dahal, R. K. R. Krishnan and B. Lussem, *Adv. Funct. Mater.*, 2021, **31**, 2004939.
21 S. Kushida, E. Smarsly, K. Yoshinaga, I. Wacker, Y. Yamamoto, R. R. Schröder and U. H. F. Bunz, *Adv. Mater.*, 2020, **33**, 2006061.
22 Y. Fu, N. Wang, A. Yang, Z. Xu, W. Zhang, H. Liu, H. K.-W. Law and F. Yan, *Anal. Chem.*, 2021, **93**, 14359–14364.
23 P. D'Angelo, S. L. Marasso, A. Verna, A. Ballesio, M. Parmeggiani, A. Sanginario, G. Tarabella, D. Demarchi, C. F. Pirri, M. Cocuzza and S. Iannotta, *Small*, 2019, **15**, 1902332.
24 N. X. Wang, A. N. Yang, Y. Fu, Y. Z. Li and F. Yan, *Acc. Chem. Res.*, 2019, **52**, 277–287.
25 E. Bihar, Y. X. Deng, T. Miyake, M. Saadaoui, G. G. Malliaras and M. Rolandi, *Sci. Rep.*, 2016, **6**, 27582.
26 G. Scheiblin, R. Coppard, R. M. Owens, P. Mailley and G. G. Malliaras, *Adv. Mater. Technol.*, 2017, **2**, 1600141.
27 C. Z. Liao, C. H. Mak, M. Zhang, H. L. W. Chan and F. Yan, *Adv. Mater.*, 2015, **27**, 676–681.
28 A. N. Yang, Y. Z. Li, C. X. Yang, Y. Fu, N. X. Wang, L. Li and F. Yan, *Adv. Mater.*, 2018, **30**, e1800051.
29 A. Koklu, S. Wustoni, V. E. Musteata, D. Ohayon, M. Moser, I. McCulloch, S. P. Nunes and S. Inal, *ACS Nano*, 2021, **15**, 8130–8141.

30 J. J. Song, P. Lin, Y. F. Ruan, W. W. Zhao, W. W. Wei, J. Hu, S. M. Ke, X. R. Zeng, J. J. Xu, H. Y. Chen, W. Ren and F. Yan, *Adv. Healthcare Mater.*, 2018, **7**, 1800536.
31 M. J. Lu, F. Z. Chen, J. Hu, H. Zhou, G. X. Chen, X. D. Yu, R. Ban, P. Lin and W. W. Zhao, *Small Struct.*, 2021, **2**, 2100087.
32 S. P. Phadatare, M. Momin, P. Nighojkar, S. Askarkar and K. K. Singh, *Adv. Pharmacol.*, 2015, **2015**, 1–12.
33 M. Azkargorta, J. Soria, A. Acera, I. Iloro and F. Elortza, *J. Proteomics*, 2017, **150**, 359–367.
34 R. Sambursky, W. F. Davitt, R. Latkany, S. Tauber, C. Starr, M. Friedberg, M. S. Dirks and M. McDonald, *JAMA Ophthalmol.*, 2013, **131**, 24–28.
35 H. R. Culver, M. E. Wechsler and N. A. Peppas, *ACS Nano*, 2018, **12**, 9342–9354.
36 P. Lin, F. Yan and H. L. W. Chan, *ACS Appl. Mater. Interfaces*, 2010, **2**, 1637–1641.
37 J. Kypr, I. Kejnovska, D. Renciuk and M. Vorlickova, *Nucleic Acids Res.*, 2009, **37**, 1713–1725.
38 C. C. Blake, D. F. Koenig, G. A. Mair, A. C. North, D. C. Phillips and V. R. Sarma, *Nature*, 1965, **206**, 757–761.
39 Y. Wei, A. A. Thyparambil and R. A. Latour, *Biochim. Biophys. Acta*, 2014, **1844**, 2331–2337.
40 N. D. Robinson, P. O. Svensson, D. Nilsson and M. Berggren, *J. Electrochem. Soc.*, 2006, **153**, H39–H44.
41 Z. J. Zhao, B. Q. Liu, C. L. Xie, Y. Ma, J. Wang, M. Liu, K. X. Yang, Y. H. Xu, J. Zhang, W. W. Li, L. Shen and F. J. Zhang, *Sci. China: Chem.*, 2021, **64**, 1302–1309.
42 D. A. Bernards and G. G. Malliaras, *Adv. Funct. Mater.*, 2007, **17**, 3538–3544.
43 D. A. Bernards, D. J. Macaya, M. Nikolou, J. A. DeFranco, S. Takamatsu and G. G. Malliaras, *J. Mater. Chem.*, 2008, **18**, 116–120.
44 H. Lin and S. C. Yiu, *Saudi J. Ophthalmol.*, 2014, **28**, 173–181.
45 G. Hernandez-Molina and T. Sanchez-Hernandez, *Semin. Arthritis Rheum.*, 2013, **42**, 627–639.